Photoionization for the ground state of Al VII from threshold to the *K* shell

Jiaolong Zeng, Jianmin Yuan, and Qisheng Lu
Department of Applied Physics, National University of Defense Technology, Changsha 410073, People's Republic of China
(Received 9 April 2001; revised manuscript received 12 June 2001; published 11 September 2001)

The photoionization cross sections of *N*-like Al VII are calculated from the first ionization threshold to 140 Ry using the *R*-matrix method. 14 target states (including 4 *K*-shell excited states) of Al VIII are included in the close-coupling calculation. The detailed structure and resonances of the cross sections across the *L*-shell and *K*-shell thresholds is described. The resonance energies and widths of some of the autoionization states are determined by analyzing the resonance structures. The results show that the autoionization width of the *K*-shell excited state of a $1s$ electron being excited into $2p$ orbital is the largest among all of the autoionization states. It is also larger than Doppler and Stark widths under a typical plasma condition. This result shows that the autoionization widths will have essential influence in simulating the x-ray transmission spectrum of Al plasma.

DOI: 10.1103/PhysRevA.64.042704 PACS number(s): 32.80.Fb, 32.80.Dz, 32.70.Jz

I. INTRODUCTION

In the past two decades there has been increased interest in the photoionization of atoms and ions. This is mainly due to the urgent need for radiative data for astrophysical applications such as in the opacity project [1,2] and the iron project [3], fusion research, and plasma diagnostics. The fundamental interest in the photoionization processes may also be a reason for this increase. Most of these efforts, either from theoretical or from experimental, has been devoted to the investigation of low-energy photoionization cross sections. The opacity project calculated a large amount of radiative data for most astrophysical abundant elements including aluminum atom and ions. The iron project calculated a large amount of radiative data for iron atoms and ions of different ionization stages. All of these accurate photoionization data were restricted to photon energies near the ionization threshold, no cross sections at higher energies were reported.

To our knowledge, only three or four papers were devoted to the photoionization of Al VII. Baliyan and Kingston [4] calculated the photoionization cross sections for the ground state of Al VII using the *R*-matrix method. Manson [5] compared their central-field results [6] with those of Baliyan and Kingston [4]. Excellent agreement was obtained between two results, except for the autoionization resonances, which were not included in the central-field model. Baliyan and Kingston used two sets of target-state wave functions, one with and the other without configuration interaction (CI), in their calculations. There was not much difference between the cross sections obtained using the two sets of wave functions and they concluded that their results were converged. They had only included up to $n=3$ orbitals for their CI calculations. This may not be sufficient since CI effects are supposed to be important for nitrogenlike Al VII and, as we shall demonstrate later, indeed they are. There is obviously a need to include more orbitals to take into account enough CI. On the other hand, although Baliyan and Kingston gave the cross sections up to photon energy 100 Ry, no data were reported for higher photon energies, which include the *K*-shell resonances. However, photoionization cross sections near this photon energy range are important to interpret the x-ray opacity or transmission of plasmas, especially for the photon energy range of the *K*-shell excitations from a $1s$ electron to the $2p$ orbital.

Many experimental efforts had been devoted to the measurements of x-ray transmission through aluminum plasmas [7–12]. Nearly all these experiments had been carried out in the energy region of the inner-shell excitations of one $1s$ electron to the $2p$ orbital. In order to simulate theoretically these x-ray transmission spectra, a lot of theoretical studies [13–17] had been carried out. But most of these calculations approximated the *K*-shell excited states as discrete transitions to obtain the *K*-shell absorption cross sections. Actually, these *K*-shell excited states are well above the ionization threshold and should be treated as photoionization processes. Recently, we [18] simulated the x-ray transmission of laser-produced Al plasmas under local thermodynamic equilibrium using detailed-term-accounting approximation. The photoabsorption cross sections were obtained using the *R*-matrix method. In order to have a complete understanding of the photoionization process of the aluminum ions, there is obviously a need to extend the calculation to the *K*-shell thresholds.

Close-coupling calculations of *K*-shell photoionization, which include inner-shell resonances, have been restricted to relatively simple systems, for example, Li I [19–22], Be I [23], B I [24], and C IV [25]. For more complex systems, the close-coupling calculations are very scarce. McLaughlin and Kirby and Gorczyca and McLaughlin [26,27] calculated the photoabsorption cross sections of atomic oxygen in the vicinity of the *K* edge. Bautista [28] obtained the photoionization cross sections of Fe XV from the first threshold to the *K*-shell thresholds. All these calculations used the *R*-matrix method.

II. THEORETICAL METHODS

The present close-coupling calculations of the photoionization of Al VII are carried out using the *R*-matrix package of Scott and Taylor [29]. The *R*-matrix method is very effective in considering the resonance structures and especially, the autoionization widths are naturally included in the calculation. In previous papers, we [25,30] have calculated the inner-shell photoionization of the ground and first excited states of lithiumlike carbon and the photodetachments of the

TABLE I. Orbital parameters of the radial wave functions of the target Al VIII.

Orbital	C_{jnl}	I_{jnl}	ξ_{jnl}	Orbital	C_{jnl}	I_{jnl}	ξ_{jnl}
3s	−0.192 12	1	12.863 47	$\overline{4s}$	−0.534 21	1	8.909 54
	0.048 15	1	13.652 45		8.397 76	2	2.887 92
	0.772 68	2	4.609 74		−8.184 59	3	4.756 08
	−0.090 64	2	10.327 91		1.732 94	4	8.743 70
	0.537 63	3	3.802 80		−1.955 91	4	3.896 49
	−1.751 34	3	3.015 86				
				$\overline{4p}$	−0.159 13	2	15.004 96
$3p$	−0.969 70	2	4.372 81		−5.345 16	3	5.572 30
	0.109 03	2	4.325 74		−0.614 37	4	3.015 32
	1.295 57	3	2.797 02		6.007 83	4	6.606 89
	0.166 52	3	6.450 88				
				$\overline{4d}$	0.276 23	3	7.401 71
$3d$	0.044 13	3	5.507 38		−0.651 13	4	3.120 86
	0.970 14	3	2.761 30		0.806 86	4	7.423 98
$\overline{4f}$	0.068 98	4	4.260 78	$\overline{5p}$	3.445 62	2	7.405 09
	0.949 17	4	7.337 05		−36.209 46	3	3.791 15
					−3.811 26	4	3.480 25
$\overline{5s}$	−1.669 59	1	8.303 38		20.890 26	5	7.122 60
	14.673 55	2	3.120 50		20.240 46	5	4.386 82
	1.167 99	3	13.665 86				
	−7.387 56	4	8.289 30	$\overline{5d}$	4.892 27	3	6.761 09
	−17.261 72	4	3.766 19		−1.973 97	4	7.118 68
	8.579 99	5	4.193 16		−2.949 81	5	10.006 09
					0.258 13	5	3.314 13

metastable $nsnp^2\ ^4P$ states of Be^-, Mg^-, and Ca^- ions using the *R*-matrix method. In an *R*-matrix calculation, the wave function of the $N+1$ electron system is given the form

$$\Psi_k(X_1 \ldots X_{N+1}) = \hat{A} \sum_{ij} c_{ijk} \Phi_i(X_1, \ldots, X_N \hat{\mathbf{r}}_{N+1} \sigma_{N+1}) \times u_{ij}(r_{N+1}) + \sum_j d_{jk} \phi_j(X_1, \ldots, X_{N+1}), \quad (1)$$

where $\hat{A}$ is the antisymmetrization operator to take the exchange effect between the target electrons and the free electron into account. X_i stands for the spatial ($\mathbf{r}_i$) and the spin (σ_i) coordinates of the ith electron. The functions $u_{ij}(r)$ under the first sum construct the basis sets for the continuum wave functions of the free electron, and Φ_i are the coupling between the target states and the angular and spin part of the free electron. The correlation functions ϕ_j in the second sum are constructed by the square integrable orbitals to account for the correlation effects not adequately considered because of the cutoff in the first sum. The square integrable orbitals are cast as linear combinations of Slater-type orbitals

$$P_{nl}(r) = \sum_j C_{jnl} r^{I_{jnl}} \exp(-\xi_{jnl} r). \quad (2)$$

The parameters ξ_{jnl} and coefficients C_{jnl} are determined by a variational optimization on the energy of a particular state, whilst the powers of rI_{jnl} remain fixed. For the present calculation, we include six real orbitals ($1s, 2s, 2p, \overline{3s}, 3p, 3d$) and four pseudo-orbitals ($\overline{4s}$, $\overline{4p}$, $\overline{4d}$, and $\overline{4f}$). The pertinent parameters ξ_{jnl} and coefficients C_{jnl} for all orbitals are obtained using the CIV3 computer code [31] according to the following rules. The $1s$, $2s$, and $2p$ orbitals are taken from those of the Hartree-Fock orbitals given by Clementi and Roetti [32] for the ground-state $2s^2 2p^2\ ^3P$ of Al VIII. The $3s$, $3p$, and $3d$ orbitals are obtained by optimizing on the $2s^2 2p 3s\ ^1P^o$, $2s^2 2p 3p\ ^3P$, and $2s^2 2p 3d\ ^3D^o$ state, respectively. The pseudo-orbitals $\overline{4s}$, $\overline{4d}$, and $\overline{4f}$ are obtained by optimizing on the ground state, while $\overline{4p}$ is obtained by optimizing on the $2s 2p^3\ ^3S^o$ state. The resulting orbital parameters of the radial functions are compiled in Table I. The appropriate *R*-matrix wave-function expansion was performed by including 14 target states of Al VIII, ten *L*-shell thresholds: $2s^2 2p^2\ ^3P$, $2s 2p^3\ ^5S^o, ^3D^o, ^3P^o, ^3S^o$, $2p^4\ ^3P$, $2s^2 2p 3s\ ^3P^o$, $2s^2 2p 3p\ ^3D, ^3S, ^3P$ and four *K*-shell thresholds: $1s 2s^2 2p^3\ ^5S^o, ^3D^o, ^3P^o$, and $^3S^o$. The CI effects are supposed to be quite important for complex systems such as nitrogenlike Al VII and carbonlike Al VIII ions. Baliyan and Kingston [4] discussed these CI effects from the Hartree-Fock and CI calculations. They can also be easily seen from the CI calculations of energy levels of Al VIII with and with-

TABLE II. Calculated energy levels (in Ry) for the target Al VIII ion relative to the ground state with (the fourth column $n=3+\overline{4}$) and without (the third column $n=3$) inclusion of $n=\overline{4}$ pseudo-orbitals. For comparison, experimental and other theoretical results (in Ry) obtained by Baliyan and Kingston [4] (BK) are also given.

			$n=3+\overline{4}$			BK	
State	Expt. [33]	$n=3$	Level	Diff. (%)	$n=3+\overline{4}+\overline{5}$	Level [4]	Diff. (%)
$2s^2 2p^2\ ^3P$	0.0	0.0	0.0	0.0	0.0	0.0	0.0
$2s2p^3\ ^5S^o$	1.1891	1.0766	1.1515	3.16	1.1534	1.1669	1.87
$2s2p^3\ ^3D^o$	2.3621	2.3537	2.3452	0.72	2.3441	2.4184	2.38
$2s2p^3\ ^3P^o$	2.7893	2.7840	2.7994	0.37	2.7962	2.8556	2.38
$2s2p^3\ ^3S^o$	3.6558	3.7120	3.6514	0.12	3.6485	3.6977	1.15
$2p^4\ ^3P$	5.5277	5.5594	5.5266	0.02	5.5244	5.7066	3.24
$2s^2 2p3s\ ^3P^o$	12.0224	12.0105	12.0257	0.03	12.0302		
$2s^2 2p3p\ ^3D$		12.6473	12.6576		12.6643		
$2s^2 2p3p\ ^3S$	12.7499	12.7289	12.7392	0.08	12.7459		
$2s^2 2p3p\ ^3P$		12.7891	12.7994		12.8058		
$1s2s^2 2p^3\ ^5S^o$		111.1505	111.1878		111.1018		
$1s2s^2 2p^3\ ^3D^o$		112.1177	112.1365		112.0967		
$1s2s^2 2p^3\ ^3S^o$		112.4230	112.3840		112.3462		
$1s2s^2 2p^3\ ^3P^o$		112.4832	112.4724		112.4541		

out the $n=\overline{4}$ orbitals. The calculated energy levels relative to the ground state are listed in Table II, along with the experimental [33] and theoretical results given by Baliyan and Kingston [4]. The third column $n=3$ presents the excitation energies with only $n=1$, 2, and 3 physical atomic orbitals and the fourth one $n=3+\overline{4}$ presents the results with $n=1$, 2, and 3 physical atomic orbitals, and $n=\overline{4}$ pseudo-orbitals. It can be easily seen from Table II that the calculated energy levels given by $n=3$ agree satisfactorily with experiment [33], but corresponding energy levels given by $n=3+\overline{4}$ agree excellently with experiment. The relative differences are less than 0.8% for the target states wherever the experimental values are available except for $2s2p^3\ ^5S^o$ (3.16%) state. More than half of them are less than 0.12%. These results show that CI effects are indeed important for Al VIII ion. Our results of the excitation energies represent a significant improvement on the work of Baliyan and Kingston [4] except for the $2s2p^3\ ^5S^o$ state. This improvement can also be seen from the calculated ionization potential (IP). The theoretical IP value of ours and that of Baliyan and Kingston are 17.7571 Ry and 17.792 Ry, respectively, while the observed value is 17.7454 Ry [33]. Our result of 17.7571 Ry is in better agreement with the observed value 17.745 Ry than that of Baliyan and Kingston. These results show that the present wave functions are adequate for the computation of the photoionization cross sections of Al VII. Present calculations use up to the $n=\overline{4}$ orbitals to include more CI. More accurate resonance energies and widths should be obtained with the improved excitation energies and ionization potential.

The *R*-matrix program were utilized by including 30 continuum orbitals for each continuum electron orbital angular momentum $l=0$, 1, 2, 3, 4, and 5, the *R*-matrix boundary was chosen to be 5.4 au. The energy mesh was taken to be 0.0001 Ry to show enough resonances. In order to take into account the resonances of the *K*-shell excited state, only one electron can be fixed in the $1s$ orbital, this will result in a too large target and $(N+1)$-electron configurations to make the calculation controllable if no restriction is made on the excitations of electrons. In the present calculation, at most two electrons can be excited from the basic configurations $2s^2 2p^2$, $2s2p^3$, and $2p^4$ for the target states of Al VIII and from the basic configurations $2s^2 2p^3$, $2s2p^4$, and $2p^5$ for Al VII ion.

III. RESULTS AND DISCUSSION

Figure 1 shows the total photoionization cross section of the $2s^2 2p^3\ ^4S^o$ ground state of Al VII from the first ionization threshold at 17.7571 to 140 Ry. The relative differences between the present calculated length and velocity forms of the cross sections are less than 6%, so only the length form is given. The complex resonance structures of the cross sections around the *L* shell at photon energy ranges of about 20–30 Ry and *K* shell at about 120–130 Ry can easily be seen. The most striking feature of the cross sections is that a broad and strong resonance exists at about 110 Ry. This is the first *K*-shell resonance that should be assigned to be $1s2s^2 2p^4\ ^4P$ autoionization state. Figure 1 also shows the cross sections from the *R*-matrix calculation of Baliyan and Kingston [4] (dashed line) and the central-field results of Reilman and Manson [6] (full circles) for the photon energy region from 60 to 100 Ry. Our results are in excellent agreement with two other theoretical results across this photon energy range.

The total cross sections from the first ionization threshold to the $2p^4\ ^3P$ threshold are shown in more detail in Fig. 2 with (a) referring to the cross sections between the $2s^2 2p^2\ ^3P$ and $2s2p^3\ ^5S^o$ thresholds, (b) between the $2s2p^3\ ^5S^o$ and $2s2p^3\ ^3P^o$ thresholds, (c) between the $2s2p^3\ ^3P^o$ and $2s2p^3\ ^3S^o$ thresholds, and (d) between the

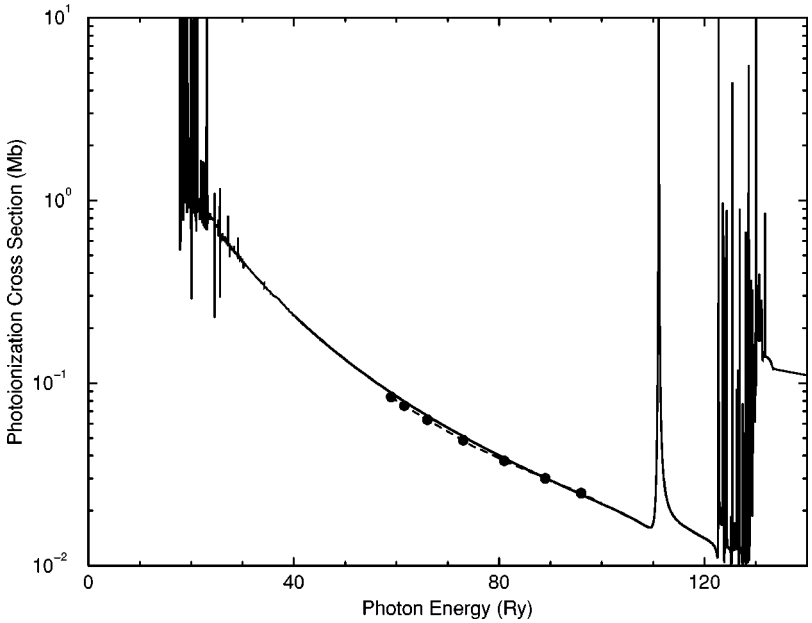

FIG. 1. Total photoionization cross sections (Mb) (in length form) of the Al VII $2s^2 2p^3\,^4S^o$ ground state. Solid line refers to the present *R*-matrix results, dashed one to the theoretical results of Baliyan and Kingston [4] and full circles to the central-field Hartree-Slater results of Ref. [6].

$2s2p^3\,^3S^o$ and $2p^4\,^3P$ thresholds of Al VIII. The structures shown in Figs. 2(a)–2(d) are rather similar to those obtained by Baliyan and Kingston [4] [Figs. 2(a)–2(d) of their paper]. Both our results and their results are dominated by the autoionization resonances between the first ionization threshold to the $2s2p^3\,^3S^o$ threshold, which are shown in Figs. 2(a)–2(c), but the resonances are much weaker between the $2s2p^3\,^3S^o$ and $2p^4\,^3P$ threshold, which is shown in Fig. 2(d). The reason is that the resonances in Figs. 2(a)–2(c) are caused by single-electron excitations, but those in Fig. 2(d)

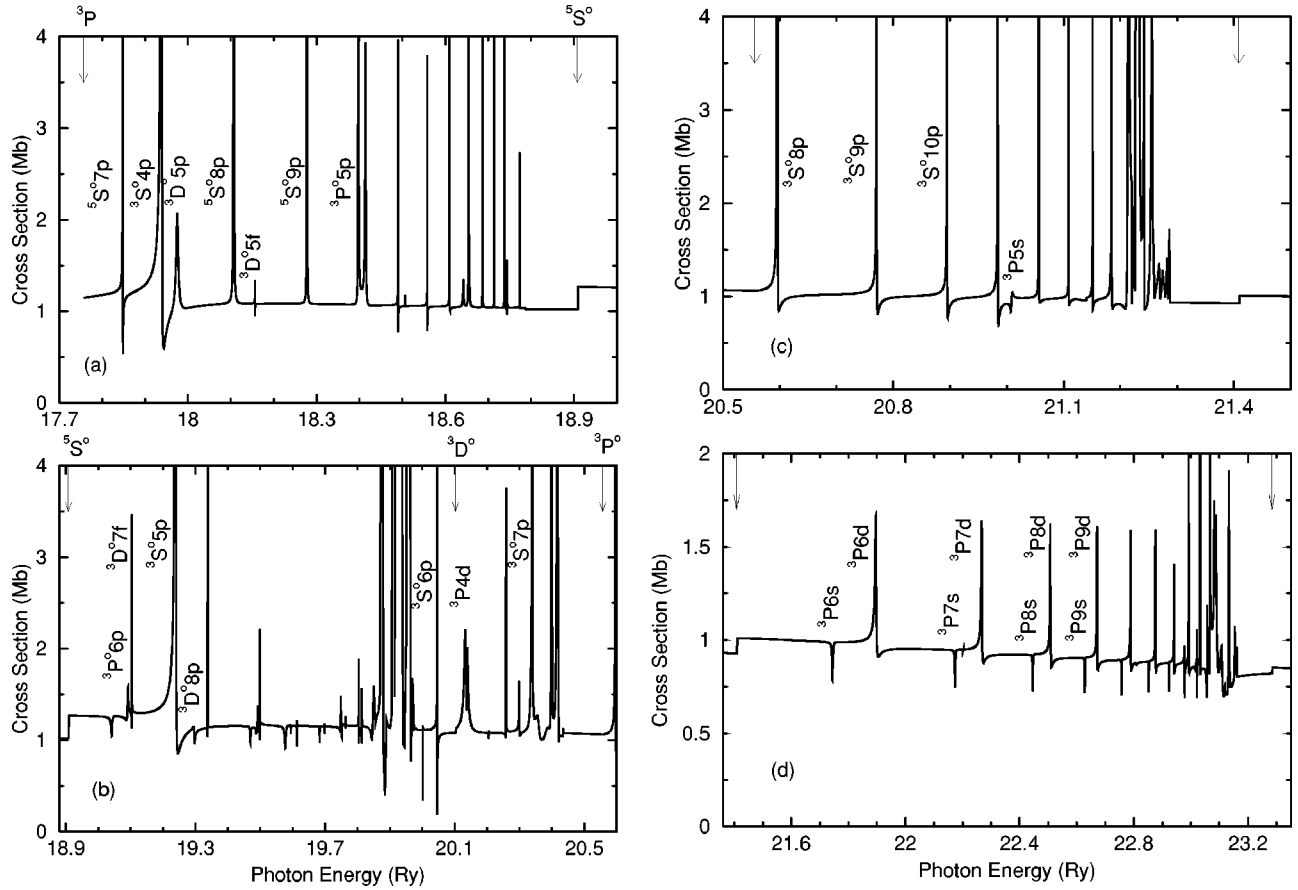

FIG. 2. Total photoionization cross sections for the Al VII $2s^2 2p^3\,^4S^o$ ground state between thresholds: (a) $2s^2 2p^2\,^3P$ and $2s2p^3\,^5S^o$, (b) $2s2p^3\,^5S^o$ and $2s2p^3\,^3P^o$, (c) $2s2p^3\,^3P^o$ and $2s2p^3\,^3S^o$, and (d) $2s2p^3\,^3S^o$ and $2p^4\,^3P$ of Al VIII ion.

TABLE III. Comparison of the resonance energies and widths (in Ry) for some autoionization states ^4P of Al VII ion between present results and those of Baliyan and Kingston (BK) [4].

Designation	Resonance energy		Resonance width	
	This work	BK	This work	BK
$2s2p^3(^5S^o)7p$	17.8483	17.9167	5.87(−4)[a]	7.043(−4)
$2s2p^3(^3S^o)4p$	17.9374	18.0021	1.28(−3)	1.194(−3)
$2s2p^3(^3D^o)5p$	17.9756	18.0308	7.56(−3)	7.763(−3)
$2s2p^3(^5S^o)8p$	18.1071	18.1763	3.42(−4)	3.302(−4)
$2s2p^3(^3D^o)5f$	18.1570	18.2221	<1.00(−4)	3.800(−6)
$2s2p^3(^5S^o)9p$	18.2789	18.3477	2.55(−4)	1.772(−4)
$2s2p^3(^3P^o)5p$	18.3979	18.4410	2.34(−3)	1.690(−3)
$2s2p^3(^3P^o)6p$	19.0911	19.1172	3.86(−3)	3.356(−3)
$2s2p^3(^3D^o)7f$	19.1045	19.1579	2.84(−4)	3.640(−4)
$2s2p^3(^3S^o)5p$	19.2368	19.2824	1.89(−3)	1.551(−3)
$2s2p^3(^3D^o)8p$	19.2948	19.3484	2.75(−3)	2.582(−3)
$2s2p^3(^3S^o)6p$	19.9207	19.9712	1.53(−3)	1.048(−3)
$2s2p^3(^3S^o)7p$	20.3387	20.3791	8.84(−4)	8.444(−4)
$2s2p^3(^3S^o)8p$	20.5953	20.6350	5.26(−4)	5.476(−4)
$2s2p^3(^3S^o)9p$	20.7703	20.8096	3.64(−4)	3.746(−4)
$2p^4(^3P)5s$	21.0561	21.0724	1.86(−3)	1.335(−3)
$2p^4(^3P)5d$	21.3012	21.3332	1.55(−3)	1.300(−3)
$2p^4(^3P)6s$	21.7438	21.7928	4.43(−3)	4.247(−3)
$2p^4(^3P)6d$	21.8959	21.9410	5.48(−3)	5.129(−3)
$2p^4(^3P)7s$	22.1747	22.2161	2.75(−3)	2.425(−3)
$2p^4(^3P)7d$	22.2684	22.3075	3.46(−3)	3.218(−3)
$2p^4(^3P)8s$	22.4470	22.4853	1.73(−3)	1.541(−3)
$2p^4(^3P)8d$	22.5071	22.5458	2.38(−3)	2.263(−3)
$2p^4(^3P)9s$	22.6291	22.6668	1.19(−3)	1.084(−3)
$2p^4(^3P)9d$	22.6715	22.7087	1.58(−3)	1.435(−3)
$1s2s^22p^4$	111.138		0.023	
$1s2s^22p^3(^5S^o)3p$	122.780		0.011	
$1s2s^22p^3(^3D^o)3p$	123.584		0.012	
$1s2s^22p^3(^3S^o)3p$	123.711		0.014	
$1s2s^22p^3(^3P^o)3p$	123.835		0.009	
$1s2s(^3S)2p^4(^3P)(^5P)3s$	124.346		0.011	
$1s2s(^1S)2p^4(^3P)(^3P)3s$	125.234		0.008	

[a]Figures in parentheses are the powers of ten by which the preceding number is multiplied.

are caused by two-electron excitations. Good agreement is also found between the background of the photoionization cross sections of two calculations. The values of the background are about 1 Mb for the two results near the ionization threshold. Above the first excited threshold $2s2p^3\,^5S^o$, the background cross sections have a little rise to about 1.2 Mb. The agreement of the structures and background cross sections between the present results and those of Baliyan and Kingston indicate that our results are reliable. The resonances above the $2p^4\,^3P$ threshold are caused by double-electron excitations and therefore, rather weak, so we do not show them in more detail.

Although good agreements are found between present results and those of Baliyan and Kingston for the structures and background cross sections, there are differences for the resonance positions between the two results. In the present paper, the resonance positions and widths are obtained by fitting a Fano profile

$$\sigma=\sigma_a+\sigma_b\frac{(q+\varepsilon)^2}{1+\varepsilon^2},$$

where σ_a and σ_b stand for constants related to the background of the resonance cross sections, respectively, $\varepsilon=2(E-E_0)/\Gamma$ with E being the photon energy, E_0 the resonance energy, Γ the resonance width, and the parameters q describes the shape of the resonance. Table III gives some resonance positions and widths with the principle quantum numbers of the valence electron being less than ten. The cross sections between the first ionization threshold and the first excited threshold, which are shown in Fig. 2(a), are dominated by the autoionization resonances belonging to the $2s2p^3(^5S^o)np$ Rydberg series. According to our calculation, the lowest three of this Rydberg series are located at 17.8483, 18.1071, and 18.2789 Ry for $n=7$, 8, and 9, respectively. The corresponding values obtained by Baliyan and Kingston

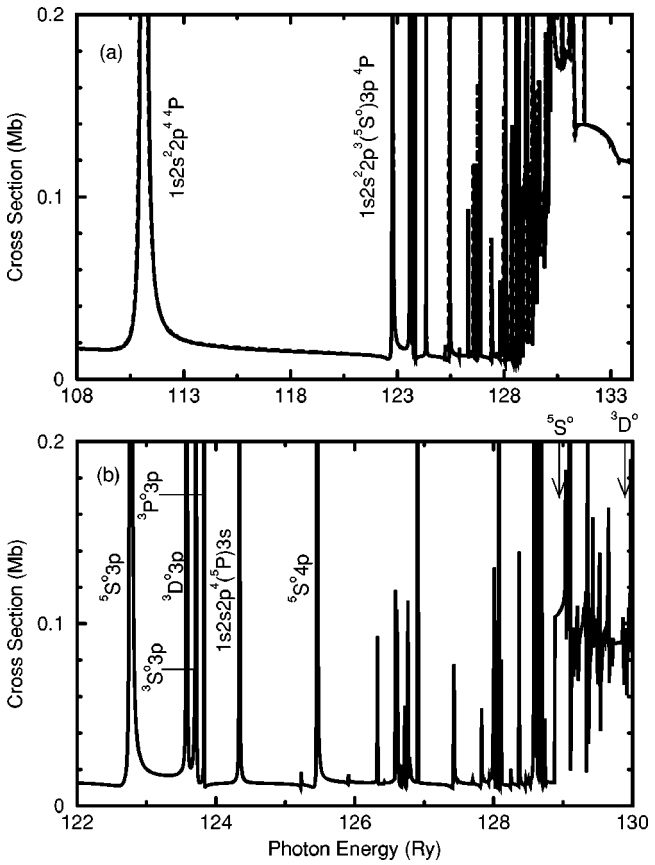

FIG. 3. Total photoionization cross sections near the *K*-shell thresholds: (a) from below the *K*-shell threshold to 140 Ry and (b) from 122 to 130 Ry. In (a), the solid line refers to the results obtained by using the wave functions constructed by $n=3+\overline{4}$ orbitals, while the dashed line to the results using the $n=3+\overline{4}+\overline{5}$ orbitals.

[4] were at 17.9167, 18.1763, and 18.3477 Ry, respectively. The resonance energies by our calculation are 0.07 Ry lower than those of Baliyan and Kingston [4]. This series is perturbed by the presence of four interlopers: $2s2p^3(^3S^o)4p$, $2s2p^3(^3D^o)5p$, $2s2p^3(^3D^o)5f$, and $2s2p^3(^3P^o)5p$ at 17.9374, 17.9756, 18.1570, and 18.3979 Ry, while the corresponding positions of the four interlopers obtained by Baliyan and Kingston [4] were at 18.002, 18.031, 18.222, and 18.441 Ry. The resonance energies of the four interlopers by our calculations are lower than those of Baliyan and Kingston. The same conclusion can be drawn for all the resonances of the Rydberg series shown in Figs. 2(b), 2(c), and 2(d). From the inspection of Table II, one can see that most resonance positions obtained by our calculation are lower than those of Baliyan and Kingston [4] by about 0.04 Ry, which is very close to the difference of IP (0.035 Ry) by the two calculations. From this comparison, we conclude that different resonance positions are mainly caused by our improved IP. As discussed above, our calculated excitation energies and IP are in better agreement with the experiment, so we conclude that our resonance positions should be more accurate.

The cross sections near the *K*-shell ionization thresholds are shown in Fig. 3, with (a) covering from below the *K*-shell threshold to $1s2s^22p^3(^3P^o)$ threshold and (b) from 122 to 130 Ry in even more detail. Several series of autoionization resonances of the kind $1s2s^22p^3(^5S^o,\ ^3D^o,\ ^3S^o,$ and $^3P^o)nl$ with $n\geqslant 3$ can be seen. These resonances rise by up to orders of magnitude above the background and contribute significantly to cross sections. This enhancement of cross sections across the *K*-shell thresholds have significant effects on the x-ray opacity or transmission over this photon energy region. The resonance energies and widths of some of these *K*-shell excited autoionization states are also given in Table III.

From the comparison of the autoionization widths given in Table III, one can find that the widest resonance is caused by the $1s2s^22p^4\,^4P$ *K*-shell excited autoionization state. We have also calculated the photoionization cross sections for some low-lying excited states of Al VII ion and find that the widths of the lowest *K*-shell excited states are also the largest among the Rydberg series. These autoionization widths have large physical effects on the x-ray opacity or transmission across this energy region. Maybe for this reason, many experimental studies on the measurements of the x-ray transmission [7–12] were devoted to this energy region of the inner-shell excitation of one $1s$ electron to the $2p$ orbital. In order to simulate theoretically these transmission spectra, one requires the resonance energies and widths of these *K*-shell excited states. In a subsequent paper, we shall give these data for the low-lying *K*-shell excited states.

In the above calculations, all the orbital functions are optimized on the valence-shell target states. There might be optimization space for the *K*-shell excited target states. To demonstrate the convergence of these *K*-shell excited states, we introduced a further set of orbitals, i.e., $\overline{5s}$, $\overline{5p}$, and $\overline{5d}$, to improve the energies of these $1s$-hole states. Three optimization schemes are performed to see the effects. The first one, $\overline{5s}$ orbital is used to minimize the energy of the $1s2s^22p^3\,^3P^o$ state, $\overline{5p}$ the $1s2s^22p^3\,^3S^o$ state and $\overline{5d}$ the $1s2s^22p^3\,^3D^o$ state. The second one, $\overline{5s}$ and $\overline{5d}$ orbitals are used to minimize the energy of the $1s2s^22p^3\,^3P^o$ state and $\overline{5p}$ the $1s2s^22p^3\,^3S^o$ state. The third one, all $\overline{5s}$, $\overline{5p}$, and $\overline{5d}$ are used to minimize the energy of the $1s2s^22p^3\ ^3P^o$ state. All three methods give rise to trivial variations of the energies of the valence-shell and the *K*-shell target states, but the second method is the most effective. The calculated target state energies are also given in Table II using the second optimization scheme. It can be seen that the energy differences between the calculations with and without $\overline{5s}$, $\overline{5p}$, and $\overline{5d}$ orbitals are small. We have recalculated the photoionization cross sections using the wave-function expansions, which include additional derived pseudo-orbitals $\overline{5s}$, $\overline{5p}$, and $\overline{5d}$. In the 17–23 Ry range of photon energy, the new cross sections are basically the same as those shown in Fig. 2. Thus, we do not give the results. In the range of inner-shell photoionization (110–130 Ry), the variations are also small. The results are shown in Fig. 3(a) with a dashed line. We believe that the differences between the calculated and experimental positions of the *K*-shell resonances are less than 0.1 Ry, at least for the $1s$-$2p$ resonance. This can be clearly demonstrated from our calculated x-ray transmission

of the Al plasma at a temperature of 40 eV and a density of 0.0135 g/cm^3 [18]. The good agreement between the calculated [18] and experimental [7,8] transmission show that the differences between the calculated and observed $1s$-$2p$ resonance energies are less than 0.1 Ry. Note that present calculations include more orbitals and thus the quality of the wave functions are better than those in our earlier work [18].

In order to simulate theoretically the transmission spectrum, one must know the line widths caused by various broadening mechanisms of the transitions. These broadening mechanisms include Doppler and Stark broadening, resonance broadening, and natural width. It is usually very difficult to consider all these broadening mechanisms in practical calculations. Which of them should be considered depend on the relative importance of these broadening mechanisms. In the past years, most theoretical simulations [13–17] only took account of Doppler broadening. This implied that autoionization widths are small compared to the Doppler or Stark broadening. However, this is not the case from the present calculation. To have a clear quantitative understanding of the autoionization widths of the lowest *K*-shell excited state, we can make a comparison among these broadening mechanisms. Because Stark widths depend on the electron density, we take the prototype experiment [7] (at a temperature of 40 eV and a density of 0.0135 g/cm^3) as an example. Under this plasma condition, one can determine the electron density to be 2.07×10^{21} cm^{-3} by solving the ionization equilibrium (Saha) equation [34]. The Stark full width at half maximum (FWHM) is estimated to be 0.04 eV$\approx$0.003 Ry for the $1s$-$2p$ transition by semiempirical method [35]. The Doppler FWHM is about 0.14 eV$\approx$0.01 Ry near the $1s$-$2p$ transition. But the autoionization width of the lowest *K*-shell excited state is 0.023 Ry$\approx$0.31 eV. This is more than twice as large as the Doppler width and larger than the Stark width by a factor of about seven. Obviously, this autoionization width is larger than the Doppler and Stark widths and therefore should be considered in simulating the x-ray transmission spectrum. The effects of the autoionization widths on the transmission spectrum of Al plasma can be seen in Ref. [18]. It was shown that better agreement with experiment can be obtained when autoionization resonance broadening is included in the calculation.

IV. CONCLUSION

The total photoionization cross sections for the Al VII ground state are calculated using the *R*-matrix method employing extensive configuration-interaction wave functions for initial and final states. More correlated orbitals are included to improve the wave functions of the target states than previous theoretical calculation. The calculated structures and background cross sections are in good agreement with other calculations below the *K*-shell threshold, but the resonance positions are systematically lower. The resonances across the inner-shell thresholds can enhance the photoionization cross sections dramatically and will contribute significantly to the x-ray opacity or transmission of the plasma. Such resonances should be considered as general features across inner-shell thresholds of all ions. The autoionization resonance energies and widths for some of the autoionization states are determined. The width of the lowest *K*-shell excited state is the largest among all the autoionization states and is also larger than the Doppler and Stark widths under typical plasma conditions. This fact shows that the autoionization width will play an important role in simulating the x-ray transmission spectrum of Al plasma.

ACKNOWLEDGMENTS

This work was supported by the National Science Fund for Distinguished Young Scholars under Grant No. 10025416, by the National Natural Science Foundation of China under Grant No. 19974075, and also by the China Research Association of Atomic and Molecular Data (CRAAMD).

[1] M. J. Seaton, J. Phys. B **20**, 6363 (1987).
[2] The Opacity Project team, *The Opacity Project* (IOP Publishing, Bristol, 1995), Vols. 1 and 2.
[3] D. G. Hummer, K. A. Berrington, W. Eissner, A. K. Pradhan, H. E. Saraph, and J. A. Tully, Astron. Astrophys. **279**, 298 (1993).
[4] K. S. Baliyan and A. E. Kingston, J. Phys. B **24**, 4743 (1991).
[5] S. T. Manson, Phys. Rev. A **46**, 2939 (1992).
[6] R. T. Reilman and S. T. Manson, Astrophys. **40**, 815 (1979).
[7] S. J. Davidson, J. M. Foster, C. C. Smith, K. A. Warburton, and S. J. Rose, Appl. Phys. Lett. **52**, 847 (1988).
[8] S. J. Davidson, C. L. S. Lewis, D. O'Neill, S. J. Rose, J. M. Foster, and C. C. Smith, in *Laser Interaction with Matter*, edited by G. Velarde, E. Minguez, and J. M. Perlado (World Scientific, Singpore, 1989).
[9] T. S. Perry, S. J. Davidson, F. J. D. Serduke, D. R. Bach, C. C. Smith, J. M. Foster, R. J. Doyas, R. A. Ward, C. A. Iglesias, F. J. Rogers, J. Jr. Abdallah, R. E. Stewart, J. D. Kilkenny, and R. W. Lee, Phys. Rev. Lett. **67**, 3784 (1991).
[10] C. A. Iglesias, M. H. Chen, D. L. McWilliams, J. K. Nash, and F. J. Rogers, J. Quant. Spectrosc. Radiat. Transf. **54**, 185 (1995).
[11] L. Aschke, S. Depierreux, K. G. Estabrook, K. B. Fournier, J. Fuches, S. Glenzer, R. W. Lee, W. Rozmus, R. S. Thoe, and P. E. Young, J. Quant. Spectrosc. Radiat. Transf. **65**, 23 (2000).
[12] C. Chenais-Popovics, F. Gilleron, M. Fajardo, H. Merdji, T. Miballa, J. C. Gauthier, P. Renaudin, S. Gary, J. Bruneau, F. Perrot, T. Blenski, W. Fölsner, and K. Eidmann, J. Quant. Spectrosc. Radiat. Transf. **65**, 117 (2000).
[13] D. P. Kilcrease, J. Jr. Abdallah, J. J. Keady, and R. E. H. Clark, J. Phys. B **26**, L717 (1993).
[14] S. J. Rose, J. Phys. B **25**, 1667 (1992).
[15] J. Jr. Abdallah and R. E. H. Clark, J. Appl. Phys. **69**, 23 (1991).
[16] C. A. Iglesias, J. K. Nash, M. H. Chen, and F. J. Rogers, J. Quant. Spectrosc. Radiat. Transf. **51**, 125 (1994).

[17] A. Rickert, J. Quant. Spectrosc. Radiat. Transf. **54**, 325 (1995); S. J. Rose, *ibid.* **51**, 317 (1994).
[18] Jiaolong Zeng, Fengtao Jin, Jianmin Yuan, Qisheng Lu, and Yongsheng Sun, Phys. Rev. E **62**, 7251 (2000).
[19] L. Voky, P. Faucher, A. Hibbert, J.-M. Li, Y.-Z. Qu, J. Yan, J. C. Chang, and F. Bely-Dubau, Phys. Rev. A **57**, 1045 (1998).
[20] L. Voky, P. Faucher, H. L. Zhou, A. Hibbert, Y.-Z. Qu, J.-M. Li, and F. Bely-Dubau, Phys. Rev. A **58**, 3688 (1998).
[21] H. L. Zhou, S. T. Manson, L. Voky, P. Faucher, F. Bely-Dubau, A. Hibbert, S. Diehl, D. Cubaynes, J.-M. Bizau, L. Journel, and F. J. Wuilleumier, Phys. Rev. A **59**, 462 (1999).
[22] H. L. Zhou, S. T. Manson, P. Faucher, and L. Voky, Phys. Rev. A **62**, 012707 (2000).
[23] K. A. Berrington, J. Pelan, and L. Quigley, J. Phys. B **30**, 4973 (1997).
[24] N. R. Badnell, D. Petrini, and S. Stoica, J. Phys. B **30**, L665 (1997).
[25] Jiaolong Zeng, Jianmin Yuan, Zhengxiu Zhao, and Qisheng Lu, Eur. Phys. J. D **11**, 167 (2000).
[26] B. M. McLaughlin and K. P. Kirby, J. Phys. B **31**, 4991 (1998).
[27] T. W. Gorczyca and B. M. McLaughlin, J. Phys. B **33**, L859 (2000).
[28] M. A. Bautista, J. Phys. B **33**, L419 (2000).
[29] N. S. Scott and K. T. Taylor, Comput. Phys. Commun. **25**, 347 (1982).
[30] Jiaolong Zeng, Jianmin Yuan, and Qisheng Lu, Phys. Rev. A **62**, 022713 (2000).
[31] A. Hibbert, Comput. Phys. Commun. **9**, 141 (1975).
[32] E. Clementi and C. Roetti, At. Data Nucl. Data Tables **14**, 177 (1974).
[33] W. C. Martin and R. Zalubas, J. Phys. Chem. Ref. Data **8**, 817 (1979).
[34] R. D. Cowan, *Theory of Atomic Spectra* (University of California Press, Berkeley, 1981).
[35] M. S. Dimitrijevic and N. Konjevic, Astron. Astrophys. **172**, 345 (1987).